

DETC2012-71294

LARGE STROKE COMB-DRIVE ACTUATORS USING REINFORCED, CLAMPED, PAIRED DOUBLE PARALLELOGRAM (C-DP-DP) FLEXURE

Mohammad Olfatnia, Siddharth Sood, Shorya Awtar*
Precision Systems Design Laboratory, Mechanical Engineering
University of Michigan, Ann Arbor, MI 48109, USA

ABSTRACT

This paper reports in-plane electrostatic comb-drive actuators with stroke as large as 245 μm , achieved by employing a novel Clamped Paired Double Parallelogram (C-DP-DP) flexure mechanism. For a given flexure beam length (L_f), comb gap (G), and actuation voltage (V), this is currently the largest comb-drive actuator stroke reported in the literature. The C-DP-DP flexure mechanism design offers high bearing direction stiffness (K_x) while maintaining low motion direction stiffness (K_y), over a large range of motion direction displacement. The resulting high (K_x / K_y) ratio mitigates the on-set of sideways snap-in instability, thereby offering significantly greater actuation stroke compared to existing designs. Further improvement is achieved by reinforcing the individual beams in this flexure mechanism. While the traditional Paired Double Parallelogram (DP-DP) flexure design with $G = 3 \mu\text{m}$, $L_f = 1 \text{ mm}$ results in a 50 μm stroke before snap-in, the reinforced C-DP-DP design with $G = 3 \mu\text{m}$ achieves a stroke of 141 μm . The same C-DP-DP flexure design provides a 215 μm stroke with $G = 4 \mu\text{m}$, and a 245 μm stroke with $G = 6 \mu\text{m}$. The presented work includes closed-form stiffness values for the reinforced C-DP-DP flexure, a design procedure for selecting dimensions of the overall comb-drive actuator, micro-fabrication of some representative actuators, and experimental measurements demonstrating the large stroke.

1. INTRODUCTION AND BACKGROUND

Electrostatic comb-drive actuators have been used in various applications such as resonators [1, 2], filters [3], micro-grippers [4], and micro/nano positioning [5-7]. A linear in-plane electrostatic comb-drive actuator comprises two electrically isolated conductive combs with N fingers each, as shown in Fig.1. While the static comb is fixed with respect to ground, the moving comb is guided via a flexure mechanism so that it can displace primarily in Y direction with respect to the static comb. These static and moving comb fingers (length L_f , in-plane thickness T_f , out-of-plane thickness H_f) have a nominal

inter-digitation gap of G and an initial engagement of Y_o . The flexure mechanism is designed to provide linear guided motion and relatively small stiffness (K_y) in the Y direction (or motion direction), along with minimal error motions (E_x) and relatively high stiffness (K_x) in the X direction (or bearing direction). In an ideal scenario, K_y and E_x would approach zero while K_x would approach infinity. However, in practice, this is never the case given the performance tradeoffs between motion range, stiffness, and error motions that exist in flexure mechanisms [8], and manufacturing imperfections that are inherent to micro-fabrication processes [9, 10]. High stiffness (K_θ) and low error motion (E_θ) are also desirable in the in-plane yaw rotation [11]. Since K_θ can be independently made large and E_θ is inherently zero for the flexure designs considered here, in-plane rotation is initially ignored. The three out-of-plane directions are also bearing directions but are less critical in the overall performance of the in-plane comb-drive actuator [12].

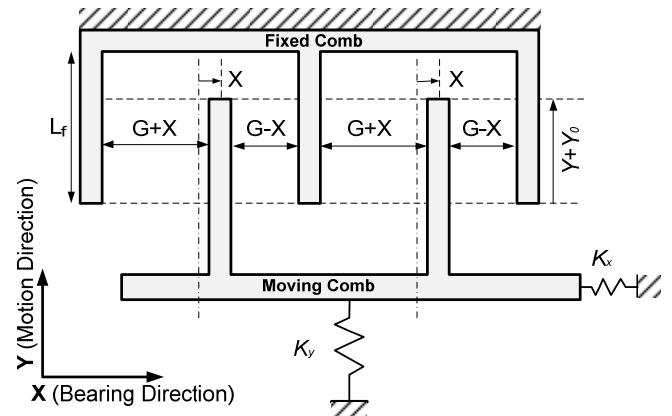


Figure 1: Schematic of an electrostatic comb drive with the springs representing the flexure bearing.

When a voltage difference (V) is applied between the two combs, they experience a mutual electrostatic attraction, which produces a displacement Y along the motion direction:

* Corresponding Author (awtar@umich.edu), 734-615-0285

$$K_y \cdot Y = \frac{\varepsilon N H_f G}{G^2 - X^2} V^2 \quad (1)$$

Here, ε is the dielectric constant of air. The bearing direction displacement X can arise due to flexure error motion, fabrication misalignment, electrostatic forces, or a possible disturbance in the X direction. While the displacement Y is dictated by the comb geometry, motion direction flexure stiffness, and the actuation voltage, its maximum stroke is limited by the snap-in phenomenon, which corresponds to sideways instability of the moving comb [13, 14]. For any Y displacement, the electrostatic force due the actuation voltage V produces a destabilizing or negative spring effect and the flexure mechanism offers stabilizing or positive spring effect in the X direction. The former increases with increasing stroke, while the latter generally reduces. The moving comb snaps sideways into the static comb at the Y displacement at which the former stiffness exceeds the latter. This condition may be mathematically expressed as [13, 15]:

$$\left(\frac{K_x}{K_y} \right) \leq \frac{2Y(Y + Y_0)}{G^2} \frac{\left(1 + \frac{3X_c^2}{G^2} \right)}{\left(1 - \frac{X_c^2}{G^2} \right)^2} \quad \text{where } E_x = \frac{4X_c^3}{G^2 + 3X_c^2} \quad (2)$$

This snap-in condition assumes that the comb-fingers are perfectly rigid and all compliance comes from the flexure. The right hand side represents a “critical stiffness ratio” needed to avoid snap-in and clearly increases with displacement Y and error motion E_x . E_x includes any motion or misalignment of the moving comb in the X direction with respect to its nominal zero position due to flexure mechanics or fabrication imperfections in the absence of electrostatic force [13]. Clearly, to delay snap-in and maximize the actuator stroke, the flexure mechanism has to provide a high (K_x/K_y) ratio that is maintained over a large range motion direction range. Since E_x is generally non-deterministic, its effect is incorporated via a positive Margin of Stability (S). Stable operation is given by:

$$\left(\frac{K_x}{K_y} \right) \geq \frac{2Y(Y + Y_0)}{G^2} (1 + S) \quad (3)$$

The paired Double Parallelogram (DP-DP) flexure mechanism has been most commonly used in electrostatic comb-drive actuators [2, 13, 14, 16-18]. While this flexure provides a high stiffness ratio (K_x/K_y) at $Y = 0$; its K_x drops precipitously with increasing Y displacements even as K_y remains largely constant. This limits the comb-driver actuator stroke due to early snap-in. Pre-bent beams in the DP-DP flexure help shift the Y displacement value at which K_x is maximum, but do not contain the drop in K_x with increasing Y [13]. This results in some improvement in the actuator stroke at the expense of robustness [15]. Other designs are successful at containing the drop in K_x stiffness with increasing Y displacement by appropriately constraining the secondary stage(s) in a DP or DP-DP flexure [19]; however, this also results in an increase in the motion direction stiffness K_y , which is undesirable.

Recently, we have proposed a new Clamped Paired Double Parallelogram (C-DP-DP) flexure mechanism, which offers high K_x over a large Y displacement range, while maintaining low K_y throughout. This new design is described in *Section 2*, along with closed-form analytical expressions for its K_x and K_y stiffness. With these improved stiffness characteristics, the C-DP-DP flexure is well suited for achieving large-stroke in comb-drive actuators. In *Section 3*, we present a step by step recipe to optimally select the dimensions of this flexure as well as the comb-drive to design an actuator with large stroke, small actuation voltage, and small footprint. Micro-fabrication of some representative actuators and experimental results are elaborated in *Section 4*. With the C-DP-DP flexure, a maximum actuation stroke of 245 μm with 1 mm flexure beam length and 6 μm comb finger gap has been demonstrated.

2. FLEXURE MECHANISM DESIGN

The paired Double Parallelogram (DP-DP) flexure is shown in Fig.2. This standard geometry, including a single DP as well as the DP-DP, has been extensively studied in the past [8, 14]. Here, we assume a general shape for each constituent beam, with two equal end-segments having uniform thickness T_1 and length $a_0 L_1$ and a rigid middle section of length $(1-2a_0)L_1$. The geometric parameter a_0 quantifies the degree of distributed compliance: $a_0=1/2$ represents a uniform thickness beam with highly distributed compliance, while smaller values of a_0 correspond to increasingly lumped compliance. This parameter allows for subsequent beam shape optimization.

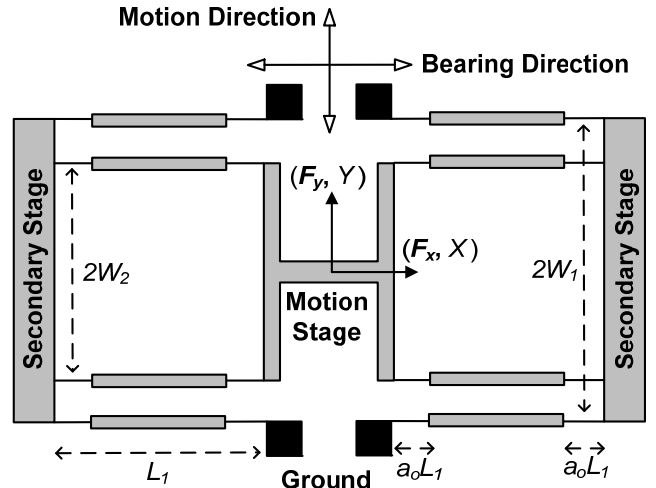


Figure 2: Paired Double Parallelogram (DP-DP) flexure

Closed-form non-linear stiffness relations for this flexure geometry have been previously derived [8] and are summarized here:

$$K_y = \frac{2EI_1}{L_1^3} \left[k_{11}^{(0)} - \frac{1}{4k_{11}^{(0)}} \left(\frac{F_x L_1^2}{EI_1} k_{11}^{(1)} \right)^2 \right] \quad (4)$$

$$K_x = \frac{2EI_1}{L_1^3} \frac{k_{33}}{\left(1 + k_{33} \left(g_{11}^{(1)} + \frac{(k_{11}^{(1)})^2}{k_{11}^{(0)}}\right) \left(\frac{Y}{2L_1}\right)^2\right)} \quad (5)$$

$$K_\theta = \frac{EI_1}{L_1^3} \cdot \frac{4W_1^2 W_2^2}{(W_1^2 + W_2^2)} \cdot \frac{k_{33}}{\left(1 + k_{33} g_{11}^{(1)} \left(\frac{Y}{2L_1}\right)^2\right)} \quad (6)$$

Here, the non-dimensional terms $k_{11}^{(0)}$, $k_{11}^{(1)}$, $g_{11}^{(1)}$, and k_{33} are all functions of the beam shape (a_o and T_l) and are referred to as beam characteristic coefficients [20]. These are graphically illustrated in Fig.3 and mathematically expressed as follows:

$$\begin{aligned} k_{11}^{(0)} &= \frac{6}{(3 - 6a_o + 4a_o^2)a_o} \\ k_{11}^{(1)} &= \frac{3(15 - 50a_o + 60a_o^2 - 24a_o^3)}{5(3 - 6a_o + 4a_o^2)^2} \\ g_{11}^{(1)} &= \frac{2a_o^3(105 - 630a_o + 1440a_o^2 - 1480a_o^3 + 576a_o^4)}{175(3 - 6a_o + 4a_o^2)^3} \\ k_{33} &= \frac{6}{a_o(T_l/L_1)^2} \end{aligned} \quad (7)$$

$k_{11}^{(0)}$ corresponds to the normalized elastic stiffness of an individual beam in the motion direction; $k_{11}^{(1)}$ corresponds to the kinematic effect of beam arc-length contraction as it bends as well as load-stiffening of the beam in the motion direction in the presence of a bearing direction force; $g_{11}^{(1)}$ corresponds to the elastokinematic effect that contributes additional bearing direction beam compliance in the presence of motion direction displacement; and k_{33} is the elastic stiffness of the individual beam normalized with respect to its bending stiffness.

As per Eq.(4), the DP-DP flexure provides a low K_y stiffness that remains constant with Y , and reduces to a simple expression in the absence of significant bearing force \mathbf{F}_x . This motion direction stiffness depends directly on $k_{11}^{(0)}$, which is insensitive to values of a_o around 0.5 but grows significantly as a_o decreases (Fig.3). This mechanism also provides a high K_x stiffness for $Y = 0$, as per Eq.(5). However, this stiffness drops precipitously with increasing Y displacement (Fig.4). Analytically, there are two sources of additional compliance, as seen in the denominator of Eq.(5). The first source arises from the elastokinematic effect manifested in the product $k_{33}g_{11}^{(1)}$, which approaches zero with reducing a_o (Fig.5). However, this is dominated by the second source that is based on the kinematic effect, manifested in the term $(k_{11}^{(1)})^2 k_{33}/k_{11}^{(0)}$. The latter is at least two orders of magnitude greater than the former, is largely insensitive to variation in a_o , and never approaches zero (Fig.5). Therefore, as seen in Fig.4, while the initial K_x / K_y ratio at $Y = 0$ can be increased by approaching

lumped compliance (i.e. lower value of a_o), the impact of this shape variation is negligible at higher Y displacements.

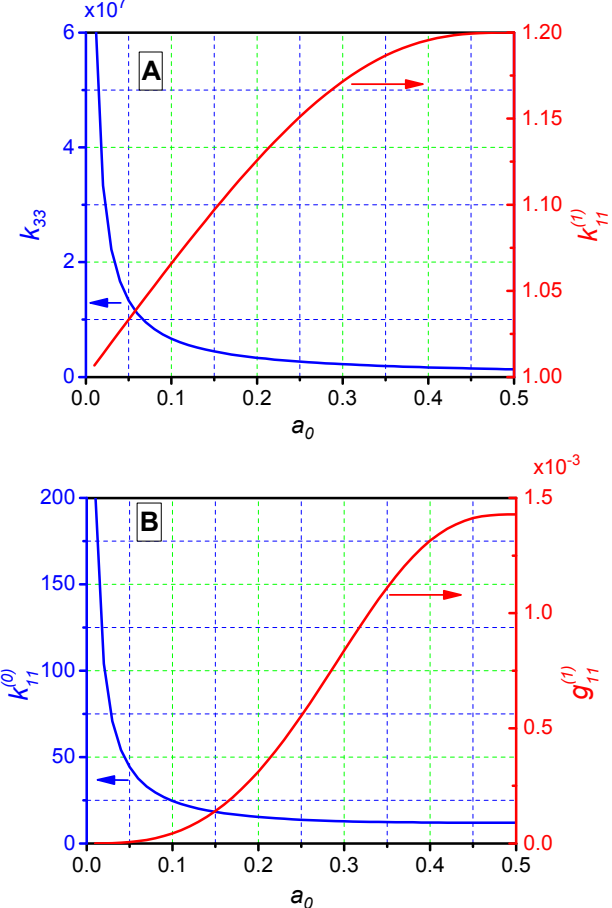


Figure 3: Beam Characteristic Coefficients. For $k_{33}, T_l/L_1$ is assumed to be 0.003.

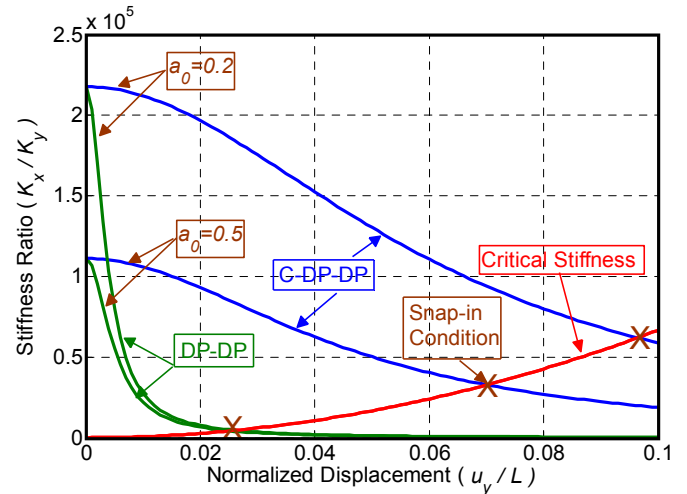


Figure 4: (K_x / K_y) stiffness ratio provided by DP-DP and C-DP-DP flexures for different values of beam reinforcement (a_o). A typical critical stiffness curve is included to demonstrate the effect of stiffness ratio on comb-drive actuator snap-in.

Qualitatively, the kinematic or load-stiffening effect is fundamental to a beam flexure and does not go away simply by beam shape optimization. The reason it plays an important role in the DP-DP flexure's bearing direction stiffness is because of the mechanism topology. In this design, the secondary stages of both the DPs are inadequately constrained in the Y direction. When the Y displacement of the motion stage is held fixed, and a small bearing direction force F_x is applied, the two secondary stages move opposite to each other in the motion direction from their nominal displacement of $Y/2$. This is because the motion direction stiffness of the each of the individual beams within the two DPs changes in the presence of F_x due to the load-stiffening effect. In the absence of this "extra" motion direction displacement of the two secondary stages, the kinematic error of the individual beams in the bearing direction no longer cancels out perfectly, thereby producing an "extra" X displacement at the motion stage and therefore lower K_x .

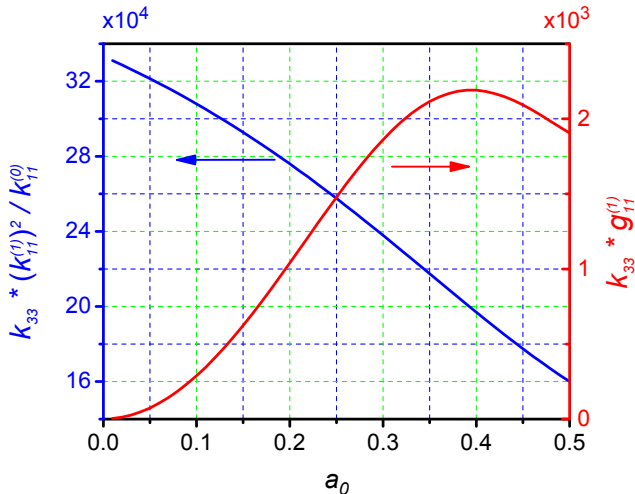


Figure 5: Elastokinematic and kinematic contributions to the bearing direction compliance of DP-DP flexure

Furthermore, as given by Eq.(6), the yaw direction stiffness (K_θ) also drops with increasing Y displacement. But since this drop is dependent only on the elastokinematic effect manifested in the product $k_{33}g_{11}^{(1)}$, the drop is relatively less and can be further restricted via smaller values of a_0 .

In order to avoid the above-described sharp decrease in the X bearing stiffness, it is desirable to constrain the Y motion of both the secondary stages such they always remain at their nominal value $Y/2$, i.e. at half of the Y motion of the motion stage. However, any topological feature that is considered to accomplish this should not restrict the small X displacements of each of these secondary stages. Restricting this X displacement, which is a kinematic component, would lead to an over-constraint in the overall flexure mechanism, resulting in very high motion direction stiffness (K_y).

We have recently proposed the Clamped Paired Double Parallelogram (C-DP-DP) flexure mechanism that accomplishes the goal of appropriately constraining the secondary stages via an external clamp as shown in Fig.6 [21].

In this design, the two secondary stages are connected to an external clamp via secondary parallelogram (P) flexures. The high rotational stiffness of these P flexures minimizes any relative Y displacement between the two secondary stages, forcing them to maintain $Y/2$ displacement at all times. This constrains these stages from responding to an X direction force on the motion stage. Also, the low X direction stiffness of the secondary P flexures offers minimal resistance to the kinematic X direction displacement of the secondary stages.

The analytical relations for the motion and bearing stiffness of the C-DP-DP flexure have been separately derived [21] and are summarized here:

$$K_y = \frac{EI_1}{L_1^3} \left(2k_{11}^{(0)} + \frac{3k_{11}^{(0)}k_{11}^{(1)}}{20} \left(\frac{L_1^3}{L_3^3} \right) \left(\frac{Y}{L_1} \right)^2 \right) \quad (8)$$

$$K_x = \frac{2EI_1}{L_1^3} \frac{k_{33}}{\left(1 + k_{33} \left(g_{11}^{(1)} + \frac{(k_{11}^{(1)})^2}{k_{11}^{(0)}(1+\eta)} \right) \left(\frac{Y}{2L_1} \right)^2 \right)} \quad (9)$$

$$\text{where, } \eta = \left(\frac{6W_3^2 L_1^3}{k_{11}^{(0)} L_2^2 L_3 T_3^2} \right)$$

The beam characteristic coefficients here are the same as earlier (Eq.(7)). Although beams in the secondary parallelograms are assumed to be of uniform thickness, it is straight-forward to introduce a separate beam shape parameter a_0' for them later, if needed [21].

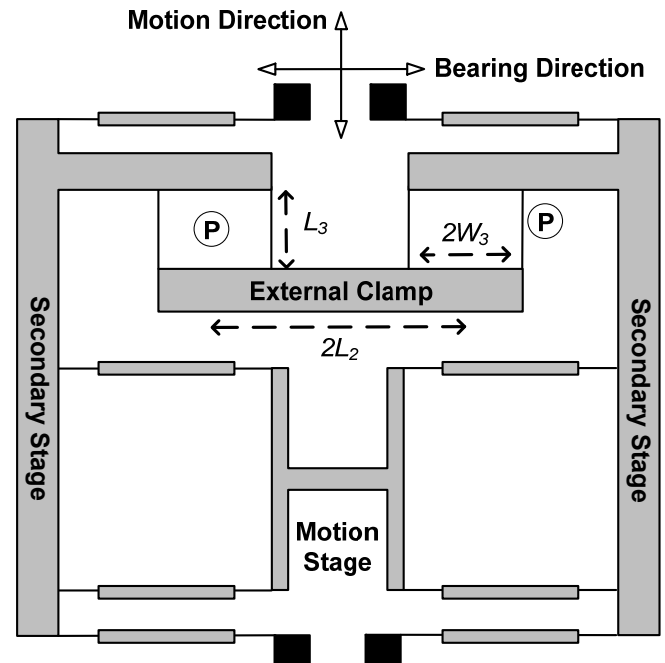


Figure 6: The Clamped paired Double Parallelogram (C-DP-DP) flexure

Eq.(8) shows that there is a slight increase in K_y because of the external clamp. However, this can be mitigated by choosing a large enough secondary parallelogram beam length L_3 . Next,

the effectiveness of the clamp in restricting the precipitous drop in the bearing direction stiffness K_x is captured via the dimensionless parameter η in Eq.(9). The external clamp prevents relative Y motion between the two secondary stages by employing the high rotational stiffness of its constituent parallelograms, which manifests itself in the form of η . For low values of W_3 , this stiffness and therefore η are small. It may be analytically seen that as $\eta \rightarrow 0$, the K_x stiffness becomes exactly the same as that for a DP-DP flexure, which corresponds to a completely ineffective clamp. However, as W_3 increases, the parameter η also increases. Eq.(9) shows that as η becomes very large, the kinematic term $(k_{11}^{(1)})^2 / k_{11}^{(0)}$ vanishes and only the

elastokinematic term $g_{11}^{(1)}$ remains. Since the latter is at least two orders of magnitude smaller than the former, this implies that the drop in K_x stiffness now is significantly reduced and that the clamp proves to be effective. Furthermore, because of the sensitivity of the elastokinematic term to beam shape, reinforced beams ($a_0 < 0.5$) may be used to produce even greater improvements in the bearing stiffness K_x of the C-DP-DP flexure. This is in contrast with the DP-DP flexure for which beam reinforcement produces marginal benefits.

The (K_x/K_y) stiffness ratio for the C-DP-DP flexure for two different values of a_0 is shown in Fig.4, which demonstrates its superior stiffness characteristics compared to the DP-DP flexure. Also shown is a representative critical stiffness ratio curve for a typical comb-drive actuator, and the resulting snap-in conditions for the flexure designs considered here.

The in-plane yaw stiffness (K_θ) of a C-DP-DP flexure with high η remains the same as that for the DP-DP, as given by Eq. (6). All the results in this section assume perfectly rigid stages, external clamp, ground anchors, and beam reinforcements. These results have been extensively validated via finite elements analysis, and reported separately [21].

3. COMB-DRIVE ACTUATOR DESIGN RECIPE

In this section, we present a systematic procedure for designing a C-DP-DP flexure based comb-drive actuator to maximize its actuation stroke while minimizing device footprint and actuation voltage. Given the several constraints and tradeoffs involved, the goal here is to obtain a good starting point for the flexure and comb-drive dimensions ($L_1, T_1, a_0, W_1, W_2, L_2, L_3, W_3, G, L_f$, and T_f) based on some simplifying assumptions, and subsequently iterate to further refine the overall design.

The following assumptions are made initially and are revisited during later design steps:

1. Analytical results in the previous section show that the optimization of the external clamp and secondary parallelograms is decoupled from the final stiffness of the C-DP-DP flexure, as long as the clamp is effective. Since an optimal clamp that provides high η can always be created subsequently, motion and bearing stiffness values corresponding to high η ($\rightarrow \infty$) are assumed at the on-set of this design procedure.

$$K_y = \frac{2EI_1 k_{11}^{(0)}}{L_1^3} \quad (10)$$

$$K_x = \frac{2EI_1}{L_1^3} \frac{k_{33}}{\left(1 + k_{33}g_{11}^{(1)}\left(\frac{Y}{2L_1}\right)^2\right)} \quad (11)$$

2. The motion stage, secondary stage, external clamp, ground anchors, and beam reinforcements are all assumed to be perfectly rigid.

3. Although the in-plane rotational stiffness (K_θ) of the C-DP-DP flexure is high, it is assumed infinity and therefore ignored in the first iteration.

4. Although the C-DP-DP flexure exhibits theoretically zero error motions in the X and Θ directions because of its inherent symmetry, misalignment and error motions due to fabrication imperfection are inevitable. Therefore, a safety margin of $S = 1$ (see Eq.(3)) is assumed to provide robustness against such non-deterministic factors.

5. Silicon is chosen as the flexure and comb-drive material, which sets an upper bound for the maximum achievable stroke due to mechanical failure. For a generalized beam flexure, the yield limit is given by [8]

$$Y_{yield} = \left(\frac{4}{k_{11}^{(0)}} \right) \left(\frac{S_y}{E} \right) \left(\frac{L_1^2}{T_1} \right) \quad (12)$$

where S_y is the yield strength and E is the Young's Modulus.

6. An initial comb-finger engagement Y_0 is needed to overcome fringing effects that are important for small Y displacements. However, Y_0 is much smaller than the maximum Y displacement and is therefore dropped in the initial steps of the design procedure.

With these assumptions in mind, one can now substitute the motion and bearing direction stiffness expressions for an optimal C-DP-DP (Eqs. (10) and (11)) into the snap-in condition (3) for a comb-drive actuator:

$$\frac{k_{33}}{k_{11}^{(0)} \left(1 + k_{33}g_{11}^{(1)}\left(\frac{Y_{max}}{2L_1}\right)^2\right)} = \frac{4Y_{max}^2}{G^2} \quad (13)$$

This snap-in condition corresponds to maximum motion direction displacement Y_{max} , which is also the actuation stroke, and associated stiffness values. The actuation voltage V_{max} at this maximum displacement may be obtained from Eq.(1):

$$NV_{max}^2 = \frac{E}{6} \left(\frac{T_1}{L_1} \right)^3 \frac{k_{11}^{(0)} Y_{max} G}{\varepsilon} \quad (14)$$

The left hand side in the above equation represents the actuation effort, which should generally be minimized. Lower N helps reduce the device foot-print and V_{max} is often restricted by practical instrumentation and operational limits.

As earlier, $k_{11}^{(0)}, g_{11}^{(1)}$, and k_{33} are all functions of a_0 and (T_1/L_1) , as given by Eq.(7). We next present a step by step recipe for choosing the dimensions of the C-DP-DP and comb-drive that employs the analytical knowledge compiled so far.

Step 1: Start with assuming a dimension for the flexure beam length L_1 , which directly impacts the device foot-print. In the first iteration, we start with a value of $L_1 = 1 \text{ mm}$.

Step 2: Minimizing the T_1/L_1 ratio lowers the actuation effort (Eq.(14)) and reduces the bending stress in the flexure beams. A smaller T_1/L_1 ratio also increases the left hand side of Eq.(13), thus delaying the snap-in condition. Therefore, the flexure beam thickness should be chosen to be a small value dictated by the practical limits of the micro-fabrication process. As mentioned in the next section, this limit is $1.7 \mu\text{m}$ in our case, and we choose $T_1 = 3 \mu\text{m}$, which corresponds to a T_1/L_1 ratio of 0.003.

Step 3: Now, the two key remaining design variables in Eqs. (13) and (14) are a_0 and G . These two equations may be solved simultaneously to eliminate G to produce:

$$NV_{\max}^2 = \frac{E}{3\varepsilon} \left(\frac{T_1}{L_1} \right)^3 Y_{\max}^2 \sqrt{\left(k_{11}^{(0)} \right)^3 \left[\frac{1}{k_{33}} + \left(\frac{Y_{\max}}{2L} \right)^2 g_{11}^{(1)} \right]} \quad (15)$$

The above condition can be plotted on an NV_{\max}^2 versus Y_{\max} graph for multiple fixed values of a_0 (Fig.7). Each solid line, referred to an *iso-a₀* line represents a fixed value of a_0 and varying values of G . Similarly, the above equations are solved to eliminate a_0 , and the resulting condition is plotted on the same NV_{\max}^2 versus Y_{\max} graph for fixed values of G . Each dashed line, referred to an *iso-G* line, represents a fixed value of G and varying values of a_0 . Moving along an *iso-a₀* line, it is clear that for a given beam shape (a_0), one can achieve higher stroke by increasing the comb-gap G , but this also increases the actuation effort NV_{\max}^2 . Similarly, moving along an *iso-G* line, one can achieve greater stroke by reducing a_0 , which once again leads to a higher actuation effort.

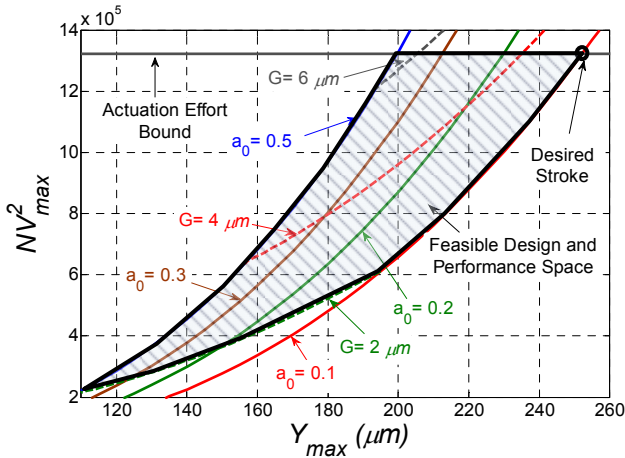


Figure 7: Design and performance space for C-DP-DP flexure based comb-drive actuators

From the design and performance space presented by Fig.7, one can graphically choose the beam shape a_0 and comb-gap G to maximize stroke while minimizing the actuation effort. There is a lower bound on G dictated by the micro-fabrication process ($2 \mu\text{m}$, in our case) and an obvious upper bound on a_0 (0.5). These bounds produce a feasible design and performance space,

represented by the shaded region in Fig.7.

Step 4: At this point, one can either set a maximum allowable actuation effort and pick the corresponding actuation stroke; or alternatively choose the desired actuation stroke and pick the actuation effort. We choose a desired actuation stroke greater than or equal to $250 \mu\text{m}$.

Step 5: For a desired stroke, clearly smaller values of a_0 and G in the feasible design space result in the lowest actuation effort. However, one has to be caution while choosing small values of these two design variables. Small a_0 leads to increasingly higher stresses in the flexure beams and the material failure becomes a concern. For a given Y_{\max} , a_0 may be chosen to maintain an adequate margin of safety against material failure using Eq. (12). Separately, the snap-in condition becomes highly sensitive to error motions E_x for very small G , and the assumed safety margin S of 1 can prove to be adequate. For our designs, we chose $a_0 = 0.2$ and G values in the range of $3\text{--}6 \mu\text{m}$.

Step 6: Having chosen a_0 and G in the previous step, we now have a numerical value of the actuation effort from Fig.7. The number of comb-fingers N can be chosen next while keeping the maximum actuation voltage V_{\max} within relevant practical limits. We selected $V_{\max} = 150\text{V}$ based on our existing instrumentation capabilities.

Step 7: One can now start to layout the flexure mechanism and the comb-drive. The dimensions W_1 and W_2 should be chosen such that rotational stiffness K_θ given by Eq.(6) is adequately high. If it is more than an order of magnitude higher than $K_x L_4^2$ at Y_{\max} , the contribution of the rotational stiffness may be ignored. Here L_4 is the distance along Y axis from the center of the flexure mechanism to the center of the comb-drive. If this condition is not met, then the rotational stiffness should be taken into account in the next iteration using a modified version of the snap-in condition [11].

Step 8: The external clamp is designed next. Using Eq.(8), choose L_3 to be large enough so that increase in the motion direction stiffness K_y due to the clamp over the above-selected Y_{\max} is within a few percent. Next, choose T_3 to be a small but practically feasible value. We choose T_3 to be equal to T_1 , i.e. $3 \mu\text{m}$. Next, choose W_3 and L_2 to make the clamp effectiveness parameter η at least 100. With an effective clamp thus designed, it can now be included in the overall device layout.

Step 9: Next, choose the in-plane thickness for the motion stage, secondary stages, and external clamp to be at least 50 times that of the flexure beams (T_1). If these dimensions are chosen to be less for whatever reason, then the contribution of these stages to the bearing direction stiffness K_x should be estimated, and a revised snap-in condition with this reduced effective K_x should be used in the next design iteration.

Step 10: Choose Y_0 to be at least 2–3 times the comb-gap G . Then, choose the comb-finger length L_f to be slightly greater than $(Y_0 + Y_{\max})$. For this comb-finger length, the comb-finger thickness T_f should be chosen to avoid local snap-in of individual finger. This is given by the following condition [22]:

$$T_f \geq \left(24 \frac{\varepsilon L_f^4}{EG^3} \frac{V_{\max}^2}{V_{PI}^2} \right)^{\frac{1}{3}}, \text{ where } V_{PI} = 3.516 \quad (16)$$

Step 11: Note that the depth of the flexure beams and comb-fingers, H_f , does not play a role in the overall actuator performance and should be selected to be large enough to avoid out-of-plane collapse during fabrication or operation.

This concludes the first iteration of the overall actuator's dimensional layout including the flexure and the comb-drive. If the device foot-print turns out to be too large or too small, one can start the process again from Step 1 with a different value of beam length L_f . Once an acceptable foot-print is achieved, a final check on the actuation, snap-in, and material failure conditions should be performed while removing the previously listed assumptions. This can lead to further refinement of the actuator dimensions. This procedure was used to design several devices that were subsequently fabricated.

4. EXPERIMENTAL RESULTS AND DISCUSSION

A. Fabrication

The comb-drive actuators were fabricated using two different process flows – surface and bulk micromachining – as shown in Fig.8. In both methods, silicon on insulator (SOI) wafers with device layer of 50 μm , buried oxide layer of 2 μm , and silicon handle layer of 350 μm were used. The device layer of these SOI wafers is heavily boron doped (P type) with resistivity of 0.001-0.005 $\Omega\text{-cm}$. In the surface micromachining based process flow, the device layer was first patterned by lithography methods, and then etched using deep reactive ion etching (DRIE). The minimum standing beam width achievable with our DRIE recipe is 1.7 μm . After this etching step, devices were diced and then released by etching the buried oxide layer using concentrated Hydrofluoric (HF) Acid (49%) at an etch-rate of 1.5 $\mu\text{m}/\text{min}$. Finally, critical point dryer was used to dry samples to avoid stiction [23]. In this drying method, liquid CO_2 is transferred to vapor via the supercritical phase (@ $T_c=38^\circ$, $P_c=80\text{atm}$) to avoid capillary forces that arise from the surface tension at the liquid-vapor interface. For this drying method to be successful, overnight soak in alcohol (e.g. methanol) before drying is recommended. With this method, devices with up to 3.5 mm suspended length were released successfully; however, the possibility of stiction remained high for actuators with 4 or 5 mm suspended lengths. To overcome this limitation, we used the second method of fabrication shown in Fig.8. In this method, the silicon handle layer was first patterned and etched by DRIE; then, the buried oxide was removed by HF etching; and, finally the device layer was patterned and etched. A scanning electron microscope (SEM) image of a representative fabricated device is shown in Fig.9.

B. Characterization

The fabricated comb-drive actuators were driven by DC voltages applied via probes at the static and moving combs. The voltage was swept to the desired maximum voltage in a ramp profile with 1 V incremental steps and 0.05 s hold time

between steps. The displacement response of the actuators was observed using an optical microscope and video-captured with a CCD camera. Subsequently, displacement measurements were extracted from the video using image processing software. These measurements were found to be repeatable within 1 μm .

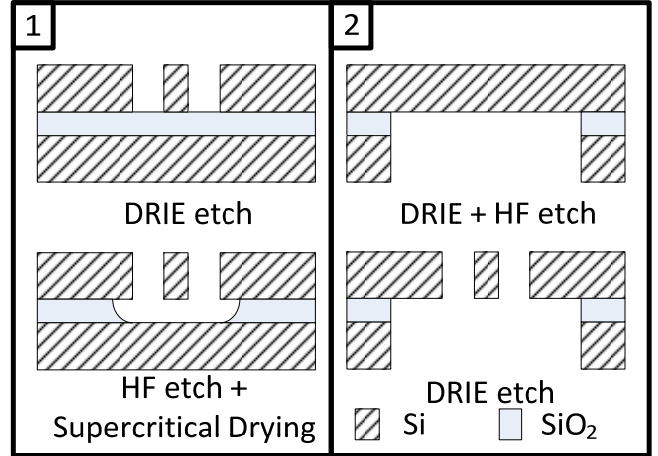


Figure 8: Fabrication process flow based on (1) surface micromachining and (2) bulk micromachining

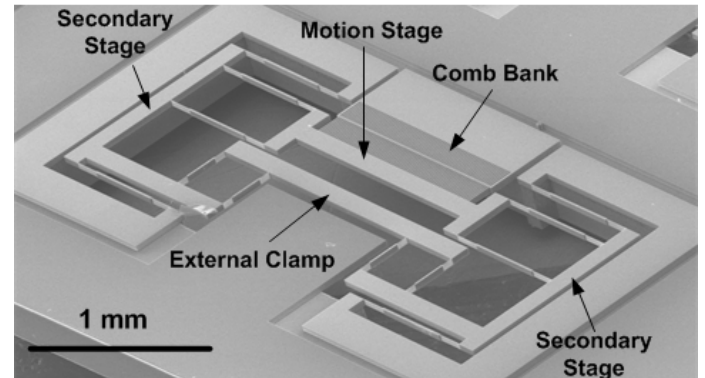


Figure 9: SEM image of a fabricated device.

C. Voltage-Stroke Curves

Fig.10 shows the displacement versus voltage curves for three different flexures with comb gap of 3 μm , beam length of 1 mm, $a_0=0.5$, and beam width of 4 μm . The measured actuator stroke using the traditional DP-DP flexure with these dimensions was 50 μm . This stroke increases to 119 μm for a C-DP-DP flexure with the same dimensions. This stroke further increases to 141 μm when reinforced beams with $a_0=0.2$ are used. This is 2.82 times higher than the actuation stroke provided by the DP-DP flexure, thus highlighting the superior performance of the reinforced C-DP-DP flexure in electrostatic comb-drive actuators.

As shown previously, the stroke of comb drive actuator can be further improved by increasing the comb gap. This is demonstrated in Fig. 11, where a stroke of 215 μm is reported for a C-DP-DP flexure with beam length of 1 mm, comb-gap of 4 μm , and $a_0 = 0.2$. The benefit of beam reinforcement is also evident here. With an identical design, the experimentally

measured stroke is 170 μm and 157 μm for $a_0=0.3$ and $a_0=0.4$, respectively. Finally, a large stroke of 245 μm at 120V for a C-DP-DP flexure with beam length of 1 mm, $a_0=0.2$, and comb gap of 6 μm is also reported on this figure. For a given flexure beam length, comb gap, and actuation voltage, this is the largest comb-drive actuator stroke reported in the literature (Fig.12), to the best of our knowledge.

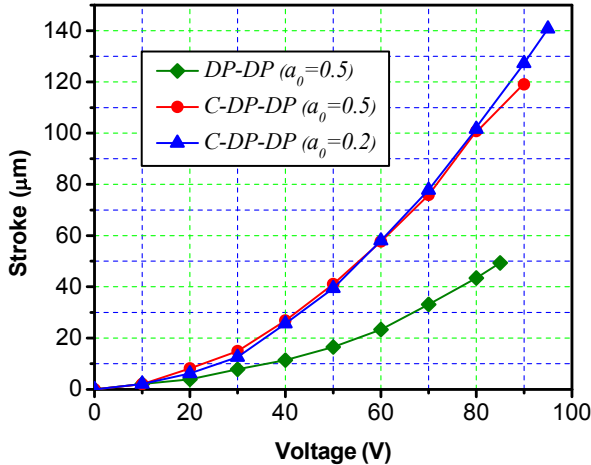


Figure 10: Displacement measurements for DP-DP and C-DP-DP flexures.

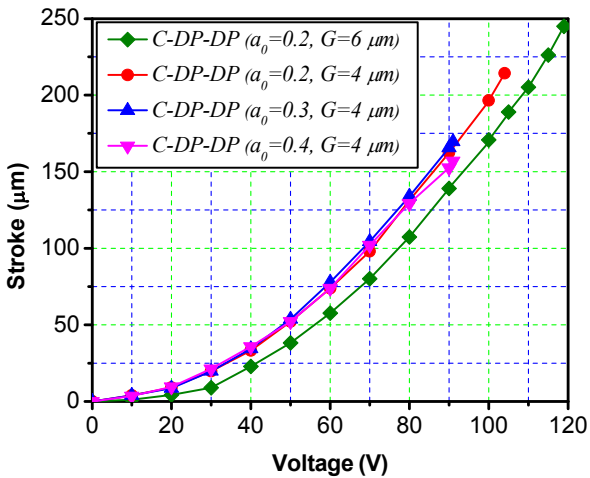


Figure 11: Displacement measurements for DP-DP and C-DP-DP flexures.

5. CONCLUSION

This paper presents the Clamped Paired Double Parallelogram (C-DP-DP) flexure mechanism with reinforced beams, which offers high bearing direction stiffness (K_x) while maintaining low motion direction stiffness (K_y), over a large range of motion direction displacement (Y). Closed-form analytical expressions for these non-linear stiffness characteristics are provided. It is shown that this flexure mechanism helps delay the on-set of snap-in instability in a comb-drive actuator and therefore provides greater actuation stroke. A systematic procedure for designing a C-DP-DP

flexure based comb-drive actuator to maximize its actuation stroke while minimizing device foot-print and actuation voltage is presented. For 1 mm flexure beam length and 6 μm comb gap, strokes as large as 245 μm have been demonstrated. This experimental proof along with the analytical formulation clearly highlights the effectiveness of the C-DP-DP flexure for large range comb-drive actuators.

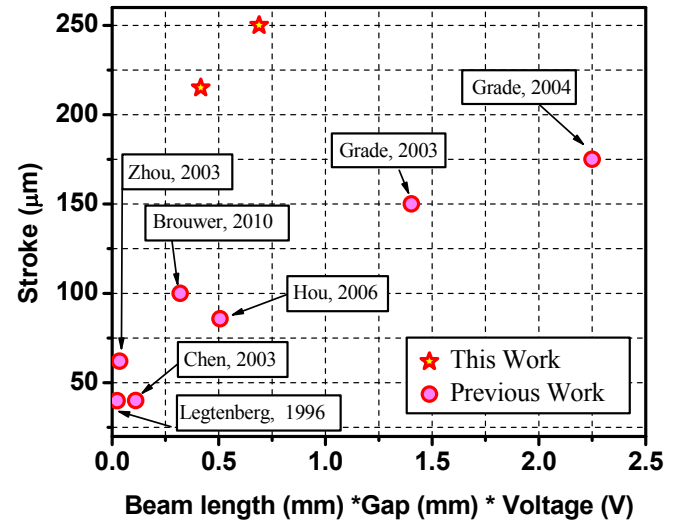


Figure 12: Comparison of our results with previously reported comb-drive actuator designs. The top-left corner, where our results lie, corresponds to large stroke, small device footprint, and small actuation voltage.

ACKNOWLEDGEMENT

The experimental portion of this work was performed at the Lurie Nanofabrication Facility, a member of the National Nanotechnology Infrastructure Network, which is supported in part by the National Science Foundation. The second author acknowledges a NIST-ARRA Measurement Science and Engineering Graduate Research Fellowship.

REFERENCES

- [1] M. W. Judy, R. T. Howe, and Ieee, *Polysilicon Hollow Beam Lateral Resonators*. New York: IEEE, 1993.
- [2] W. C. Tang, T. C. H. Nguyen, and R. T. Howe, "Laterally Driven Polysilicon Resonant Microstructures," *Sensors and Actuators*, vol. 20, pp. 25-32, 1989.
- [3] L. W. Lin, C. T. C. Nguyen, R. T. Howe, and A. P. Pisano, *Microelectromechanical Filters for Signal-Processing*, 1992.
- [4] K. Chang-Jin, A. P. Pisano, and R. S. Muller, "Overhung electrostatic microgripper," in *Solid-State Sensors and Actuators, 1991. Digest of Technical Papers, TRANSDUCERS '91.. 1991 International Conference on*, 1991, pp. 610-613.
- [5] J. D. Grade, K. Y. Yasumura, and H. Jerman, "Advanced, vibration-resistant, comb-drive actuators for use in a

- tunable laser source," *Sensors and Actuators a-Physical*, vol. 114, pp. 413-422, Sep 2004.
- [6] L. J. Ji, Y. Zhu, S. O. R. Moheimani, M. R. Yuce, and Ieee, "A Micromachined 2DOF Nanopositioner with Integrated Capacitive Displacement Sensor," in *2010 Ieee Sensors*, ed, pp. 1464-1467.
- [7] D. M. Brouwer, B. R. de Jong, and H. Soemers, "Design and modeling of a six DOFs MEMS-based precision manipulator," *Precision Engineering-Journal of the International Societies for Precision Engineering and Nanotechnology*, vol. 34, pp. 307-319.
- [8] S. Awtar, A. H. Slocum, and E. Sevincer, "Characteristics of beam-based flexure modules," *Journal of Mechanical Design*, vol. 129, pp. 625-639, Jun 2007.
- [9] B. T. Chen and J. M. Miao, "Influence of deep RIE tolerances on comb-drive actuator performance," *Journal of Physics D-Applied Physics*, vol. 40, pp. 970-976, Feb 21 2007.
- [10] K. Chen, A. Ayun, X. Zhang, and S. Spearing, "Effect of process parameters on the surface morphology and mechanical performance of silicon structures after deep reactive ion etching (DRIE)," *Journal of Microelectromechanical Systems*, vol. 11, pp. 264-275, 2002.
- [11] W. Huang and G. Y. Lu, "Analysis of lateral instability of in-plane comb drive MEMS actuators based on a two-dimensional model," *Sensors and Actuators a-Physical*, vol. 113, pp. 78-85, Jun 15 2004.
- [12] D. M. Brouwer, "Design principles for six degrees-of-freedom MEMS-based precision manipulators," University of Twente, 2007.
- [13] J. D. Grade, H. Jerman, and T. W. Kenny, "Design of large deflection electrostatic actuators," *Journal of Microelectromechanical Systems*, vol. 12, pp. 335-343, 2003.
- [14] R. Legtenberg, A. W. Groeneveld, and M. Elwenspoek, "Comb-drive actuators for large displacements," *Journal of Micromechanics and Microengineering*, vol. 6, pp. 320-329, 1996.
- [15] S. Awtar and T. Trutna, "An Enhanced Stability Model for Electrostatic Comb-Drive Actuator Design," in *Proc. IDETC/CIE*, Montreal, Canada, 2010.
- [16] G. Y. Zhou and P. Dowd, "Tilted folded-beam suspension for extending the stable travel range of comb-drive actuators," *Journal of Micromechanics and Microengineering*, vol. 13, pp. 178-183, Mar 2003.
- [17] M. T. K. Hou, G. K. W. Huang, J. Y. Huang, K. M. Liao, R. S. Chen, and J. L. A. Yeh, "Extending displacements of comb drive actuators by adding secondary comb electrodes," *Journal of Micromechanics and Microengineering*, vol. 16, pp. 684-691, Apr 2006.
- [18] C. C. Chen, C. Lee, Y. J. Lai, and W. C. Chen, "Development and application of lateral comb-drive actuator," *Japanese Journal of Applied Physics Part 1-Regular Papers Short Notes & Review Papers*, vol. 42, pp. 4059-4062, 2003.
- [19] D. M. Brouwer, A. Otten, J. B. C. Engelen, B. Krijnen, and H. M. J. R. Soemers, "Long-range Elastic Guidance Mechanisms for Electrostatic Comb-drive Actuators," in *Proceedings of the EUSPEN International Conference*, Delft, 2010.
- [20] S. Awtar, K. Shimotsu, and S. Sen, "Elastic Averaging in Flexure Mechanisms: A Three-Beam Parallelogram Flexure Case Study," *Journal of Mechanisms and Robotics-Transactions of the Asme*, vol. 2, Nov 2010.
- [21] S. Sood and S. Awtar, "Clamped Symmetric Double Parallelogram Flexure Mechanism with Improved Bearing Performance," in *Review of Scientific Instruments*, ed.
- [22] D. Elata and V. Leus, "How slender can comb-drive fingers be?," *Journal of Micromechanics and Microengineering*, vol. 15, pp. 1055-1059, May 2005.
- [23] N. Tas, T. Sonnenberg, H. Jansen, R. Legtenberg, and M. Elwenspoek, "Stiction in surface micromachining," *Journal of Micromechanics and Microengineering*, vol. 6, pp. 385-397, Dec 1996.